

PCCP

Accepted Manuscript



This is an *Accepted Manuscript*, which has been through the Royal Society of Chemistry peer review process and has been accepted for publication.

Accepted Manuscripts are published online shortly after acceptance, before technical editing, formatting and proof reading. Using this free service, authors can make their results available to the community, in citable form, before we publish the edited article. We will replace this *Accepted Manuscript* with the edited and formatted *Advance Article* as soon as it is available.

You can find more information about *Accepted Manuscripts* in the [Information for Authors](#).

Please note that technical editing may introduce minor changes to the text and/or graphics, which may alter content. The journal's standard [Terms & Conditions](#) and the [Ethical guidelines](#) still apply. In no event shall the Royal Society of Chemistry be held responsible for any errors or omissions in this *Accepted Manuscript* or any consequences arising from the use of any information it contains.

On the Structural Stability of Ionic Liquid/IRMOF Composites: A Computational Study

Hadi Abroshan^a and Hyung J. Kim^{a, b, c, *}

^aDepartment of Chemistry, Carnegie Mellon University, Pittsburgh, Pennsylvania 15213, United States

^bSchool of Computational Sciences, Korea Institute for Advanced Study, Seoul 130-722, Korea

*Corresponding Author: E-mail: hjkim@cmu.edu.

^cPermanent Address: Carnegie Mellon University

Abstract

Structural stability of isorecticular metal organic frameworks, IRMOF-1 and IRMOF-10, confining ionic liquids (ILs) inside their nano-porous cavities is studied via molecular dynamics (MD) simulations. Imidazolium- and pyridinium-based ILs, including BMI⁺PF₆⁻, BMI⁺Br⁻, BMI⁺Tf₂N⁻, BMI⁺DCA⁻, and BuPy⁺Tf₂N⁻ (BMI⁺ = 1-butyl-3-methylimidazolium, PF₆⁻ = hexafluorophosphate, Br⁻ = bromide, Tf₂N⁻ = bis(trifluoromethylsulfonyl)imide, DCA⁻ = dicyanamide, and BuPy⁺ = N-butylpyridinium), at different loadings are considered. It is found that both IRMOFs are structurally unstable and deform dramatically from their crystal structure in the presence of ILs. The interactions between the metallic parts of IRMOF and IL anions play a major role in structural disruption and collapse of these MOFs. Thus elongated anions such as Tf₂N⁻ and DCA⁻ that can interact with two different metal sites tend to lower IRMOF stability compared to spherical anions Br⁻ and PF₆⁻. A further analysis via density functional theory (DFT) and *ab initio* molecular dynamics (AIMD) simulations lends support to the MD results for structural instability of IRMOFs in the presence of ILs.

Keywords: IRMOF-1, Ionic Liquid, molecular dynamics simulation, DFT calculations, *ab initio* molecular dynamics, structural stability

Introduction

Metal-organic frameworks (MOFs) are a relatively new class of nano-porous materials in which metallic components are connected together by organic molecules, called “linkers”. The use of different building blocks---both metallic parts and linkers of varying lengths with differing functional groups---results in a wide range of different types of MOFs, which vary substantially in geometries and pore size, and thus their physicochemical properties.^{1,2} Thanks to their large surface areas, adjustable pore size and controllable pore surface properties, IRMOFs, consisting of zinc oxide clusters (Zn_4O) connected by organic linkers, have been studied extensively for applications such as gas storage and separation. One important example is CO_2 capture, which has received special attention because of concerns over greenhouse gas emissions and global warming issues.³⁻⁷

ILs have gained overwhelming interest over the last decade or so due to their attractive properties, such as low melting points, non-volatility, non-flammability as well as good thermal and chemical stability.^{8,9} It has been shown that ILs have good potential for adsorbing and separating CO_2 from a gas mixture.¹⁰ Nevertheless, high viscosity of ILs poses a significant barrier to the diffusion of adsorbates in ILs. This drawback can be partially addressed by utilizing ILs supported in cavities of porous solids.¹¹ Compared with neat ILs, supported IL phase reduces the ILs’ viscosity and improves the mechanical strength and separation efficiency.^{11,12} Recent molecular simulations by Jiang and co-workers^{13,14} suggest that ILs supported in IRMOF-1 (in which the linker is 1,4-benzenedicarboxylate) might be useful for CO_2 capture. Their study also indicates that the increase in the IL concentration in the IL/IRMOF-1 composites may improve CO_2 selectivity, i.e., enhancement of CO_2 adsorption from a CO_2/N_2 mixture.

Another interesting application of ILs in connection with MOFs is ionothermal synthesis advanced by Morris and co-workers.^{15,16} With ILs used as a solvent and a template/structure-directing agent in materials synthesis, ionothermal synthesis offers a versatile and promising approach to prepare many different types of solids, including novel MOFs.¹⁷⁻²³ As such, it has received increasing attention as a robust pathway towards synthesizing new solids and hence advancing functional materials.²⁴⁻²⁷ Because of ILs’ roles both as the spectator solvent and as the active reactants, structural building blocks, and charge-compensating groups, they can influence and even govern the final crystal structure and morphologies of solids. In this context, the

molecular-level insight on IL-solid interactions is important to understand structure and stability of the materials, such as MOF in ILs.

Computer simulations are a useful method to probe and analyze IL-MOF interactions. MOFs are often treated as non-dissociable frameworks in simulation studies although in reality, they are flexible and dissociable. One important consequence of flexible and dissociable frameworks is capturing of molecules that are larger than MOF pore dimension, e.g., toluene inside nickel-pyridine MOF.²⁸ Another is structural and chemical instability of IRMOFs. For instance, IRMOFs are vulnerable to humid air²⁹⁻³³ and quick hydrolysis of their frameworks leads to a dramatic drop in surface area.^{33,34} Since these features cannot be accounted for with a non-dissociable model,^{13,14} it is both worthwhile and desirable to re-examine IRMOFs in the presence of ILs using a flexible and dissociable description and compare with the predictions of the non-dissociable model. There are a few flexible force field descriptions³⁵⁻⁴⁴ that correctly capture a range of structural properties of MOFs, such as thermal expansion, elastic moduli, and vibrational spectra as well as guest dynamics. In this paper, we examine the structural stability of IRMOF-1 and IRMOF-10 in the presence of ILs via MD using the force-field description proposed by Greathouse and Allendorf.³⁵ To assess the results obtained with classical MD, a further analysis via DFT and *ab initio* molecular dynamics simulations is performed. Our study shows that in the presence of ILs, IRMOF structure is unstable or, at least, highly prone to undergo major changes. This finding indicates that IRMOFs may not provide a viable system to support ILs inside their pores.

The outline of this paper is as follows: The models and methods employed in simulations and DFT calculations are first described briefly. The results for MOF structure in the presence of ILs are discussed next. Concluding remarks are offered at the end.

Simulation Method

MD simulations. The unit cell of IRMOF-1 was adopted from its crystal structure with the lattice spacing 25.67 Å.⁴⁵ A $2 \times 2 \times 2$ supercell of this framework with a total of 8 unit cells (see Figure S1 in Supporting Information) was constructed and an IL was placed inside the supercell. In addition to imidazolium-based ILs that allow a direct comparison with earlier work with a non-dissociable MOF description,^{13,14} pyridinium-based ILs are considered. We varied the number of guest ion pairs in the supercell to examine the effect of IL concentration on the MOF

stability (see Table 1). For each system, energy optimization, *NVT* annealing from 800 K to 300 K, and equilibration were first conducted in the presence of rigid MOF structure. This was followed by energy minimization on the entire system (MOF + IL) using a dissociable MOF description. MD simulations were carried out for 10 ns on the resulting structure using *NPT* ensemble at 1 *atm* and 300 K. All simulations were performed using the NAMD package.⁴⁶ The Langevin dynamics and Nose-Hoover Langevin piston were used to keep the temperature and pressure constant, respectively.⁴⁷ No symmetry constraints were applied, so that lattice parameters were allowed to change in each direction independently. The particle mesh Ewald (PME) algorithm was used to calculate the long-range electrostatic interactions.⁴⁸ The van der Waals forces were truncated using a cutoff of 12 Å. Short and long range energy terms were calculated every 0.5 fs and 1.0 fs, respectively. The potential model based on OPLS-AA was employed to describe interactions involving ILs.⁴⁹⁻⁵² We note parenthetically that structure of ILs inside carbon nanotubes was studied previously using the same model description.^{53,54} For IRMOF, we employed both the dissociable and non-dissociable force field descriptions of ref 35. The dissociable description,³⁵ based on the CVFF force field combined with non-bonded parameterization of ZnO, successfully predicts⁵⁵ collapse of MOF above a critical water concentration in concert with experiments.³³

DFT calculations. A zinc oxide cluster (Zn_4O) coordinated by six formate (HCO_2^-) anions was used as a model IRMOF system for DFT calculations (Figure 1). Its molecular structure in the absence and presence of IL ions was optimized via DFT using the B3LYP hybrid functional in all-electron 6-31G(d,p) basis set.⁵⁶⁻⁵⁹ According to a prior study, this method predicts MOF structures reasonably.³⁷ A vibrational frequency analysis was performed to ensure that optimized structures we obtained are stable states, corresponding to local energy minima. All calculations were carried out with the Gaussian 09 package.⁵⁹

Ab initio molecular dynamics. For efficient computations, we considered a model unit cell consisting of 83 atoms, in which 1,4-benzenedicarboxylate linkers of IRMOF-1 are replaced by 4,4'-biphenyldicarboxylate (Figure 2). (For comparison, an IRMOF-1 unit cell contains 424 atoms.⁴⁵) We note that this model system resembles IRMOF-10 but its torsional angle between two biphenyl groups is initially set at 90° (see Figure S2 in Supporting Information). This system was simulated via AIMD in the absence and presence of a guest IL ion pair for 3.5 ps and 4.2 ps, respectively, in the *NPT* ensemble at 1 *atm* and 300 K. The Vanderbilt Ultra-Soft method was

used to describe the interaction between the electrons and nuclei.^{60,61} The Perdew–Burke–Ernzerhof (PBE) form of the generalized gradient approximation was employed for electron exchange and correlation.^{62,63} The Grimme-D2 method was used to incorporate the van der Waals (vdW) interactions into the system with a cutoff of 12 Å.⁶⁴ All calculations were carried out with the Quantum Espresso 5.1 package.⁶⁵

Results and discussions

Classical MD simulations. MD results for IRMOF-1 structure in the presence of ILs are compiled in Table 1. The most noteworthy aspect there is that IRMOF-1 is not stable. For all ILs we studied, the IRMOF-1 structure was found to collapse completely at IL loadings as low as about 15 ion pairs in the simulation supercell consisting of 8 MOF unit cells. We do not exclude the possibility that some of the stable MOF systems in Table 1 could become unstable if simulations are performed considerably longer than 10 ns. This finding calls into question the use of rigid or non-dissociable force field parameters for IRMOFs to study their interactions with ILs.

The radial distribution functions (RDFs) of anions around Zn in Figure 3 show pronounced peak structures at small r . This means that many of the anions are situated close to Zn_4O sites of MOF and interact with its zinc atoms, in agreement with previous results obtained with a rigid MOF description.^{13,14} Interestingly, the RDF peaks in the dissociable MOF description are located at considerably smaller separations than those in the rigid model. This attributed to the displacement of Zn atoms from their equilibrium positions in the dissociable model (cf. Figure 4). These structural changes allow IL anions to access Zn atom sites better and more easily (because steric hindrance arising from other moieties of the MOF is reduced) than in the rigid model description. We also mention that IL ions show an inhomogeneous distribution, clustered near the MOF skeleton in a very non-uniform manner (see Figure S1). Some MOF unit cells are occupied by multiple ion pairs, while some other cells are totally unoccupied.

Another interesting result is that the critical IL density for structural instability of IRMOF-1 varies with the IL's anionic species. Specifically, for given cationic species BMI^+ , the critical density tends to be lower with anions with an elongated structure. This trend is ascribed to interactions of elongated anions with multiple Zn_4O sites. To illustrate this point, two frequently occurring configurations of Tf_2N^- ions near Zn_4O sites are exhibited in Figure 5. Due

to its extended structure, Tf_2N^- can interact with Zn atoms of two different Zn_4O sites simultaneously via its O atoms with a partial negative charge. This strongly suggests that the effectiveness of Tf_2N^- in interacting with and thus disrupting the structure of metal centers is higher than that of smaller spherical anions such as PF_6^- and Br^- . We also notice in Table 1 that DCA^- is more effective in dissolving IRMOF-1 than Tf_2N^- . This is expected because the magnitude of the negative partial charge on two terminal nitrogen sites (-0.76e) of DCA^- is substantially higher than that on oxygen sites (-0.53e) of Tf_2N^- , and as a result, electrostatic interactions of the former with Zn atoms are stronger than those of the latter.

Our findings above indicate that interactions of IL anions with MOF play an important role in driving structural instability of IRMOF-1. Nonetheless, distributions of cations (Figure S3 in Supporting Information) suggest that they also contribute to MOF collapse by interacting with, in particular, O atoms of the linkers. This explains why IRMOF-1 is more stable with $\text{BuPy}^+\text{Tf}_2\text{N}^-$ than with $\text{BMI}^+\text{Tf}_2\text{N}^-$. Since the magnitude of atomic partial charges of BuPy^+ is generally smaller than that of BMI^+ , the cation-linker electrostatic interactions are weaker for the former than for the latter.

In addition to the ILs listed in Table 1, we have studied IRMOF-1 stability in the presence of other ionic liquids consisting of tetrafluoroborate, acetate or cyclopentadienyl anions paired with either BMI^+ or BuPy^+ cations. With 17 ion pairs of these ILs present inside the simulation supercell, IRMOF-1 was found to be unstable in all cases.

For insight into the dependence of the MOF stability results on IL potential models, we have considered another model for $\text{BMI}^+\text{PF}_6^-$, viz., the force field parameterization proposed by Bhargave and Balarsubramanian.⁶⁶ Its main difference from the model description of refs 49-51 is the total ionic charge. Specifically, partial charges of the cations and anions are scaled by 0.8, so that their respective total charges are 0.8e and -0.8e in the model description of ref 66. The MD results obtained with these reduced ion charges are summarized in Table 1. We notice that the critical density for the collapse of IRMOF-1 structure increases to 37 ion pairs with reduced IL charges from 17 with full charges. This clearly demonstrates the importance of MOF-IL electrostatic interactions in governing MOF structural stability. Nevertheless, IRMOF-1 becomes unstable even in the case of reduced charges *with significantly weakened electrostatic interactions*, suggesting that IRMOF structural instability we have found in the presence of ILs is independent of the details of the IL potential models.

Turning to IRMOF-10,⁵ whose 4,4'-biphenyldicarboxylate linkers afford bigger pores than 1,4-benzenedicarboxylate linkers of IRMOF-1, we considered two different loadings of $\text{BMI}^+\text{PF}_6^-$, 70 and 140 ion pairs, in its $(2 \times 2 \times 2)$ supercell. We found that in both cases, IRMOF-10 is structurally unstable just like IRMOF-1. This seems to suggest that IRMOFs are generally unstable in the presence of ILs regardless of their pore size.

We briefly pause here for perspective. While MD provides key molecular-level information on structural stability of IRMOF systems in the presence of ILs, several important features, e.g., variations of partial charges of Zn and other moieties of MOF as they deform, are not included in the MOF model³⁵ used in our study. A similar polarizability effect associated with guest molecules (ILs in our case) is also not accounted for. According to a prior study, the neglect of electronic polarizability can lead to a substantial underestimation of transport coefficients; e.g., the simulated diffusion coefficient of guest molecules like benzene was found to be an order of magnitude lower than experimental results.³⁵ Since our model description is classical, chemical reactivity, such as electron and proton transfers, is also not properly accounted for. Another potential difficulty is the combination of OPLS-AA-based parameters (ILs) with CVFF-based parameters (MOFs) invoked in our simulations.³⁹ While we do not believe any of these assumptions/approximations would have significant impact on our main result, i.e., structural instability of IRMOF in the presence of ILs, we have nonetheless attempted to address them using the DFT and *ab initio* MD methods. We turn to them next.

DFT calculations. DFT calculations were performed for $\text{Zn}_4\text{O}(\text{HCO}_2)_6$ (Figure 1) as a model fragment of IRMOF-1 in the absence and presence of 1,3-dimethylimidazolium (DMI^+) cations and Br^- , SCN^- , BF_4^- , and PF_6^- anions. As presented in Table S1 and Figure S4 in Supporting Information, calculated structural parameters of the MOF fragment in the absence of ILs are in reasonable agreement with previous theoretical and experimental results.^{37, 67, 68}

DFT calculations predict that structure of the $\text{Zn}_4\text{O}(\text{HCO}_2)_6$ fragment does not deform significantly in the presence of a DMI^+ ion whose ring hydrogen atoms interact primarily with the linkers' oxygen atoms. While Zn-O bond lengths do change somewhat compared to an isolated fragment, the tetrahedral symmetry of four O atoms coordinating a Zn atom (Figure 1) remains largely intact (see Figure S5 in Supporting Information).

When the $\text{Zn}_4\text{O}(\text{HCO}_2)_6$ fragment is exposed to an anion, however, the latter interacts directly with one of Zn atoms of the former and becomes coordinated with that Zn atom. This

increases the coordination number of the Zn atom to five (or higher) from four, resulting in a significant structural change of the Zn site. The optimized structure of the MOF fragment in the presence of one Br^- ion is displayed in Figure 6. Br^- forms a coordinate bond with one of Zn atoms with bond length of 2.333 Å. This Zn- Br^- interaction deforms the tetrahedral (T_d) structure of the Zn atom's coordination shell (Figure 1) in the crystalline phase to almost a trigonal bipyramidal (T_b) structure with Br^- as an equatorial ligand as illustrated in Figure 6b. This confirms the MD result above that Zn mainly interacts with IL anions. In the case of BF_4^- , two of its F atoms can interact with the same Zn atom, resulting in the coordination number of six for Zn (Figure S4). Depending on electronegativity of the coordinating atom of the anions, the new ligand, i.e., anion, would prefer equatorial or axial positions of T_b structure (Figure S6). For instance, in the case of SCN^- , the highly electronegative nitrogen atom acts as an axial ligand.

While addition of a DMI^+ cation to $\text{Zn}_4\text{O}(\text{HCO}_2)_6\text{-Br}^-$ complex in Figure 6 does not introduce significant structural changes, addition of a second Br^- , which forms a coordinate bond with another Zn atom, does. Upon sequential introduction of first Br^- , first DMI^+ , second Br^- and second DMI^+ ions to the $\text{Zn}_4\text{O}(\text{HCO}_2)_6$ fragment, the minimal RMSD (root mean square deviation) from its gas-phase structure generally increases as 0.597, 0.567, 0.830, and 0.839 Å according to DFT. This lends support to our MD results that interactions of anions with zinc oxide clusters (Zn_4O) are mainly responsible for deformation of IRMOF structure and that IRMOF is not stable in the presence of ILs.

Ab initio molecular dynamics. Though DFT calculations provide atomistic insights into molecular geometry of IRMOF's metallic part in the presence of ILs, the influence of system dynamics and of MOF's structural connectivity on its deformation is not included. To understand these effects, we simulated the model IRMOF system in Figure 2 with the *ab initio* method in the absence and presence of a guest ion pair DMI^+Br^- .

The AIMD results for temporal variations of the unit-cell volume of the IRMOF system are shown in Figure 7. In the case of pure MOF with no guest ion pair, its volume fluctuates but does not appear to shift with time. The average volume of the model IRMOF remains unchanged at around 5105 Å³ with lattice parameter $a = 17.2$ Å and unit-cell parameters $\alpha = \beta = \gamma \sim 90^\circ$. We parenthetically note that since the unit-cell of the actual IRMOF-10 is eight times larger than that of our model, our simulations yield 40840 Å³ and 34.4 Å for the unit-cell volume and lattice

parameter for IRMOF-10, respectively. These values compare well with the experimental results, 40285.52 Å³ and 34.28 Å.⁵

In the presence of an ion pair DMI⁺Br⁻, the model IRMOF system shows an oscillatory but steady decrease in volume. During the 4.2 ps simulation period, the volume decreases by nearly 30% from ~5100 Å³ to ~3600 Å³! Final values of its unit-cell parameters at the end of the simulation are $\alpha \sim 111^\circ$, $\beta \sim 91^\circ$ and $\gamma \sim 83^\circ$, which differ markedly from their initial values $\alpha = \beta = \gamma = 90^\circ$. Thus IRMOF structure loses its original symmetry and rapidly turns into a rhombus shape in the presence of a guest ion pair. This is in striking contrast with pure IRMOF, which retains its crystal structure throughout the simulation. (Final configurations of AIMD simulations in the absence and presence of the ion pair are displayed, respectively, in Figures S7 and S8 in the Supporting Information.) Though our AIMD simulation was performed only for a short period of time, it strongly indicates the onset of collapse or major re-structuring of MOF framework in the presence of ILs, consonant with the classical MD results presented above.

For insights into the mechanism of IL-induced disruption on MOF structure, we monitored positions of the DMI⁺Br⁻ ion pair with respect to MOF. We found that anion Br⁻ gradually moves from its initial position (> 4 Å from Zn atoms) towards the metallic part of MOF to form a bond with one of the Zn atoms. The formation of this bond induces the elongation of the bonds between Zn and three O atoms of the linkers and deforms the metallic center from its tetrahedral shape. This finding is in line with the DFT (Figure 6) and classical MD results discussed above. It also indicates that despite their limitations imposed by various approximations, our classical MD results on MOF structural stability are robust.

Concluding Remarks

In this article, we have investigated structural stability of IRMOF-1 and IRMOF-10 in the presence of ILs via classical and *ab initio* molecular dynamics simulations as well as DFT calculations. It was found that the original IRMOF structure is not stable in the presence of ILs. Both simulation and DFT results suggest that interactions between IL anions and Zn atoms of MOF play a central role in engendering structural instability of IRMOF. Therefore, elongated anions, such as Tf₂N⁻ and DCA⁻, which can interact with multiple Zn atoms, are very effective in destabilizing MOF structure, compared to spherical anions, e.g., Br⁻ and PF₆⁻. Our analysis clearly indicates that IRMOF does not offer a good support system for ILs. It also exposes the

limitations of non-dissociable force field models in describing MOF structure and dynamics in the presence of guest molecules/ions that interact strongly with MOF via Coulomb forces.

Acknowledgments

This work was supported in part by NSF Grant No. CHE-1223988.

Supporting Information

References

- 1) S. L. James, *Chem. Soc. Rev.*, 2003, **32**, 276- 288.
- 2) S. Kitagawa, R. Kitaura and S. Noro, *Angew. Chem., Int. Ed.*, 2004, **43**, 2334- 2375.
- 3) J. L. C. Rowsell and O. M. Yaghi, *Microporous Mesoporous Mater.*, 2004, **73**, 3- 14.
- 4) J.L.C. Rowsell and O.M. Yaghi, *Angew. Chem. Int. Ed.*, 2005, **44**, 4670- 4679.
- 5) M. Eddaoudi, J. Kim, N. Rosi, D. Vodak, J. Wachter, M. O'Keeffe and O. M. Yaghi, *Science*, 2002, **295**, 469- 472.
- 6) J. M. Hicks, C. Desgranges and J. Delhommelle, *J. Phys. Chem. C*, 2012, **116**, 22938- 22946.
- 7) O. M. Yaghi, M. O'Keeffe, N. W. Ockwig, H. K. Chae, M. Eddaoudi and J. Kim, *Nature* 2003, **423**, 705- 714.
- 8) S. D. Zhu, Y. X. Wu, Q. M. Chen, Z. N. Yu, C. W. Wang, S. W. Jin, Y. G. Ding and G. Wu, *Green Chem.*, 2006, **8**, 325- 327.
- 9) N. V. Plechkova and K. R. Seddon, *Chem. Soc. Rev.*, 2008, **37**, 123- 150.
- 10) M. J. Muldoon, S. N. V. K. Aki, J. L. Anderson, J. K. Dixon and J. F. Brennecke, *J. Phys. Chem. B*, 2007, **111**, 9001- 9009.
- 11) L. J. Lozano, C. Godinez, A. P. de los Rios, F. J. Hernandez-Fernandez, S. Sanchez-Segado and F. J. Alguacil, *J. Membr. Sci.*, 2011, **376**, 1-14.
- 12) R. D. Noble and D. L. Gin, *J. Membr. Sci.*, 2011, **369**, 1-4.
- 13) Y. Chen, Z. Hu, K. M. Gupta and J. Jiang, *J. Phys. Chem. C*, 2011, **115**, 21736- 21742.
- 14) K. M. Gupta, Y. Chen, Z. Hu and J. Jiang, *Phys. Chem. Chem. Phys.*, 2012, **14**, 5785- 5794.
- 15) E. R. Parnham and R. E. Morris, *Acc. Chem. Res.*, 2007, **40**, 1005–1013.

- 16) E. R. Cooper, C. D. Andrews, P. S. Wheatley, P. B. Webb, P. Wormald and R. E. Morris, *Nature*, 2004, **430**, 1012–1016.
- 17) K. Jin, X. Huang, L. Pan, J. Li, A. Appel and S. Wherland, *Chem. Commun.*, 2002, **23**, 2872–2873.
- 18) Z. J. Lin, D.S. Wragg, J. E. Warren and R. E. Morris, *J. Am. Chem. Soc.*, 2007, **129**, 10334–10335.
- 19) K. Pierre, A. Markus and T. Arne, *Angew. Chem. Int. Ed.*, 2008, **47**, 3450–3453.
- 20) H. S. Liu, Y. Q. Lan and S. L. Li, *Cryst. Growth Des.*, 2010, **10**, 5221–5226.
- 21) M. Wang, L. Long, R. Huang and L. Zheng, *Chem. Commun.*, 2011, **47**, 9834–9836.
- 22) L. Peng, J. L. Zhang, J. S. Li, B. X. Han, Z. M. Xue and G. Y. Yang, *Chem. Commun.*, 2012, **48**, 8688–8690.
- 23) L. Xu, Y. Kwon, B.D. Castro and L. Cunha-Silva, *Cryst. Growth Des.*, 2013, **13**, 1260–1266.
- 24) W. M. Reichert, J. D. Holbrey, K. B. Vigour, T. D. Morgan, G. A. Broker and R. D. Rogers, *Chem. Commun.*, 2006, **46**, 4767–4779.
- 25) J. Zhang, S. M. Chen and X. H. Bu, *Angew. Chem., Int. Ed.*, 2008, **47**, 5434–5437.
- 26) L. Liu, Y. Li, H. B. Wei, M. Dong, J. G. Wang, A. M. Z. Slawin, J. P. Li, J. X. Dong and R. E. Morris, *Angew. Chem., Int. Ed.*, 2009, **48**, 2206–2209.
- 27) Z. Ma, J. H. Yu and S. Dai, *Adv. Mater.*, 2010, **22**, 261–285.
- 28) E. J. Cussen, J. B. Claridge, M. J. Rosseinsky and C. J. Kepert, *J. Am. Chem. Soc.* 2002, **124**, 9574–9581.
- 29) J. M. Taylor, K. W. Dawson and G. K. H. Shimizu, *J. Am. Chem. Soc.*, 2013, **135**, 1193–1196.
- 30) J. Yang, A. Grzech, F. M. Mulder and T. J. Dingemans, *Chem. Commun.*, 2011, **47**, 5244–5246.
- 31) N. C. Burtch, H. Jasuja and K. S. Walton, *Chem. Rev.*, 2014, **114**, 10575–10612.
- 32) S. S. Kaye, A. Daily, O. M. Yaghi and J. R. Long, *J. Am. Chem. Soc.*, 2007, **129**, 14176–14177.
- 33) L. Huang, H. Wang, J. Chen, Z. Wang, J. Sun, D. Zhao and Y. Yan, *Microporous Mesoporous Mater.*, 2003, **58**, 105–114.
- 34) S. S. Han, S. H. Choi and A. C. T. Van Duin, *Chem. Commun.*, 2010, **46**, 5713–5715.

- 35) J. A. Greathouse and M. D. Allendorf, *J. Phys. Chem. C*, 2008, **112**, 5795- 5802.
- 36) S. Amirjalayer, M. Tafipolsky and R. Schmid, *Angew. Chem., Int. Ed.*, 2007, **46**, 463-466.
- 37) M. Tafipolsky, S. Amirjalayer and R. Schmid, *J. Comput. Chem.*, 2007, **28**, 1169-1176.
- 38) B. L. Huang, A. J. H. McGaughey and M. Kaviani, *Int. J. Heat and Mass Transfer*, 2007, **50**, 393-404.
- 39) D. Dubbeldam, K. S. Walton, D. E. Ellis and R. Q. Snurr, *Angew. Chem. Int. Ed.*, 2007, **46**, 4496–4499.
- 40) D. Farrusseng, C. Daniel, C. Gaudillère, U. Ravon, Y. Schuurman, C. Mirodatos, D. Dubbeldam, H. Frost and R. Q. Snurr, *Langmuir*, 2009, **25**, 7383–7388.
- 41) D. Raymand, A. C. T. Van Duin, D. Spångberg, W. A. Goddard III and K. Hermansson, *Surf. Sci.*, 2010, **604**, 741-876.
- 42) M. Wehring, J. Gascon, D. Dubbeldam, F. Kapteijn, R. Q. Snurr and F. Stallmach, *J. Phys. Chem. C*, 2010, **114**, 10527–10534.
- 43) D. C. Ford, D. Dubbeldam, R. Q. Snurr, V. Künzel, M. Wehring, F. Stallmach, J. Kärger and U. Müller, *J. Phys. Chem. Lett.*, 2012, **3**, 930–933.
- 44) S. Bureekaew, S. Amirjalayer, M. Tafipolsky, C. Spickermann, T. K. Roy and R. Schmid, *Physica Status Solidi (B) Basic Research*, 2013, **250**, 1128-1141.
- 45) H. Li, M. Eddaoudi, M. O’Keeffe and O. M. Yaghi, *Nature*, 1999, **402**, 276 -279.
- 46) J. C. Phillips, R. Braun, W. Wang, J. Gumbart, E. Tajkhorshid, E. Villa, C. Chipot, R. D. Skeel, L. Kale and K. Schulten, *J. Comput. Chem.*, 2005, **26**, 1781–1802.
- 47) S. E. Feller, Y. H. Zhang, R. W. Pastor and B. R. Brooks, *J. Chem. Phys.*, 1995, **103**, 4613-4621.
- 48) T. Darden, D. York and L. Pedersen, *L. J. Chem. Phys.*, 1993, **98**, 10089-10092.
- 49) J. N. Canongia Lopes, J. Deschamps and A. A. H. Pádua, *J. Chem. Phys. B*, 2004, **108**, 2038-2047.
- 50) J. N. Canongia Lopes, J. Deschamps and A. A. H. Pádua, *J. Chem. Phys. B*, 2004, **108**, 11250.
- 51) J. N. Canongia Lopes and A. A. H. Pádua, *J. Phys. Chem. B*, 2004, **108**, 16893-16898.
- 52) J. N. Canongia Lopes and A. A. H. Pádua, *J. Phys. Chem. B*, 2006, **110**, 19586-19592.
- 53) Y. Shim and H. J. Kim, *ACS Nano*, 2009, **3**, 1683–1702.

- 54) Y. Shim and H. J. Kim, *ACS Nano*, 2010, **4**, 2345–2355.
- 55) J. A. Greathouse and M. D. Allendorf, *J. Am. Chem. Soc.*, 2006, **128**, 10678-10679.
- 56) A. D. Becke, *Phys. Rev. A*, 1988, **38**, 3098-3100.
- 57) A. D. Becke, *J. Chem. Phys.*, 1993, **98**, 5648-5652.
- 58) C. Lee, W. Yang and R. G. Parr, *Phys. Rev. B.*, 1988, **37**, 785-789.
- 59) M. J. Frisch, G. W. Trucks, H. B. Schlegel, G. E. Scuseria, M. A. Robb, J. R. Cheeseman, G. Scalmani, V. Barone, B. Mennucci, G. A. Petersson, H. Nakatsuji, M. Caricato, X. Li, H. P. Hratchian, A. F. Izmaylov, J. Bloino, G. Zheng, J. L. Sonnenberg, M. Hada, M. Ehara, K. Toyota, R. Fukuda, J. Hasegawa, M. Ishida, T. Nakajima, Y. Honda, O. Kitao, H. Nakai, T. Vreven, J. A. Montgomery, Jr., J. E. Peralta, F. Ogliaro, M. Bearpark, J. J. Heyd, E. Brothers, K. N. Kudin, V. N. Staroverov, R. Kobayashi, J. Normand, K. Raghavachari, A. Rendell, J. C. Burant, S. S. Iyengar, J. Tomasi, M. Cossi, N. Rega, J. M. Millam, M. Klene, J. E. Knox, J. B. Cross, V. Bakken, C. Adamo, J. Jaramillo, R. Gomperts, R. E. Stratmann, O. Yazyev, A. J. Austin, R. Cammi, C. Pomelli, J. W. Ochterski, R. L. Martin, K. Morokuma, V. G. Zakrzewski, G. A. Voth, P. Salvador, J. J. Dannenberg, S. Dapprich, A. D. Daniels, Ö. Farkas, J. B. Foresman, J. V. Ortiz, J. Cioslowski, and D. J. Fox, Gaussian, Inc., Wallingford CT, 2009.
- 60) D. Vanderbilt, *Phys. Rev. B*, 1990, **41**, 7892-7895.
- 61) G. Kresse and J. Hafner, *J. Phys.: Condens. Matter*, 1994, **6**, 8245.
- 62) J. P. Perdew, K. Burke and M. Ernzerhof, *Phys. Rev. Lett.*, 1996, **77**, 3865-3868.
- 63) J. P. Perdew, K. Burke and M. Ernzerhof, *Phys. Rev. Lett.*, 1997, **78**, 1396-1396.
- 64) S. J. Grimme, *Comput. Chem.*, 2006, **27**, 1787-1799.
- 65) P. Giannozzi, S. Baroni, N. Bonini, M. Calandra, R. Car, C. Cavazzoni, D. Ceresoli, G. L. Chiarotti, M. Cococcioni, I. Dabo, A. Dal Corso, S. Fabris, G. Fratesi, S. de Gironcoli, R. Gebauer, U. Gerstmann, C. Gougoussis, A. Kokalj, M. Lazzeri, L. Martin-Samos, N. Marzari, F. Mauri, R. Mazzarello, S. Paolini, A. Pasquarello, L. Paulatto, C. Sbraccia, S. Scandolo, G. Sclauzero, A. P. Seitsonen, A. Smogunov, P. Umari and R. M. Wentzcovitch, *J. Phys.: Condens. Matter*, 2009, **21**, 395502–395521.
- 66) B. L. Bhargava and S. Balasubramanian, *J. Chem. Phys.*, 2007, **127**, 114510.
- 67) W. Clegg, D. R. Harbron, C. D. Homan, P. A. Hunt, I. R. Little and B. P. Straughan, *Inorg. Chim. Acta.*, 1991, **186**, 51-60.

68) M. C. Yin, C. W. Wang, C. C. Al, L. J. Yuan and J. T. Sun, *Wuhan. Univ. J. Nat. Sci.* 2004, **9**, 939-942.

Table 1. IRMOF-1 stability in the presence of guest ion pairs in the simulation supercell.^a

Number of ion pairs	BMI ⁺ PF ₆ ⁻	BMI ⁺ Br ⁻	BMI ⁺ Tf ₂ N ⁻	BMI ⁺ DCA ⁻	BuPy ⁺ Tf ₂ N ⁻	BMI ⁺ PF ₆ ^{-*}
7	S	S	S	S	S	S
9	S	S	S	NS	S	S
11	S	S	S	NS	S	S
13	S	S	NS	NS	S	S
15	NS	NS	NS	NS	NS	S
17	NS	NS	NS	NS	NS	S
35	NS	NS	NS	NS	NS	S
37	NS	NS	NS	NS	NS	NS

^a S (NS) denotes that the MOF/IL system is stable (unstable). Calculated lattice parameter of pure IRMOF-1 is 25.61 ± 0.03 Å.

*Results obtained with the force field parameterization of ref 66.

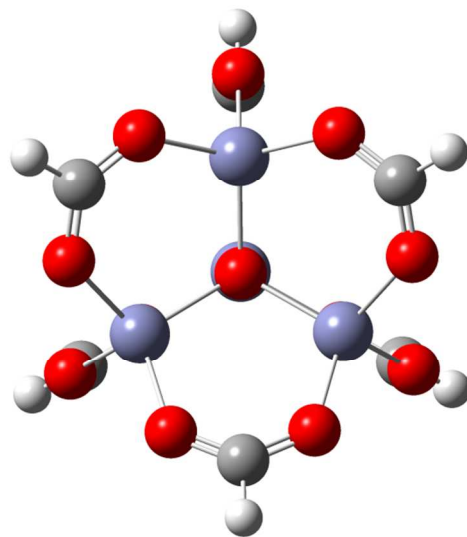


Figure 1. Molecular structure of $\text{Zn}_4\text{O}(\text{HCO}_2)_6$. Zinc, oxygen, carbon, and hydrogen atoms are shown in purple, red, dark gray and light gray, respectively.

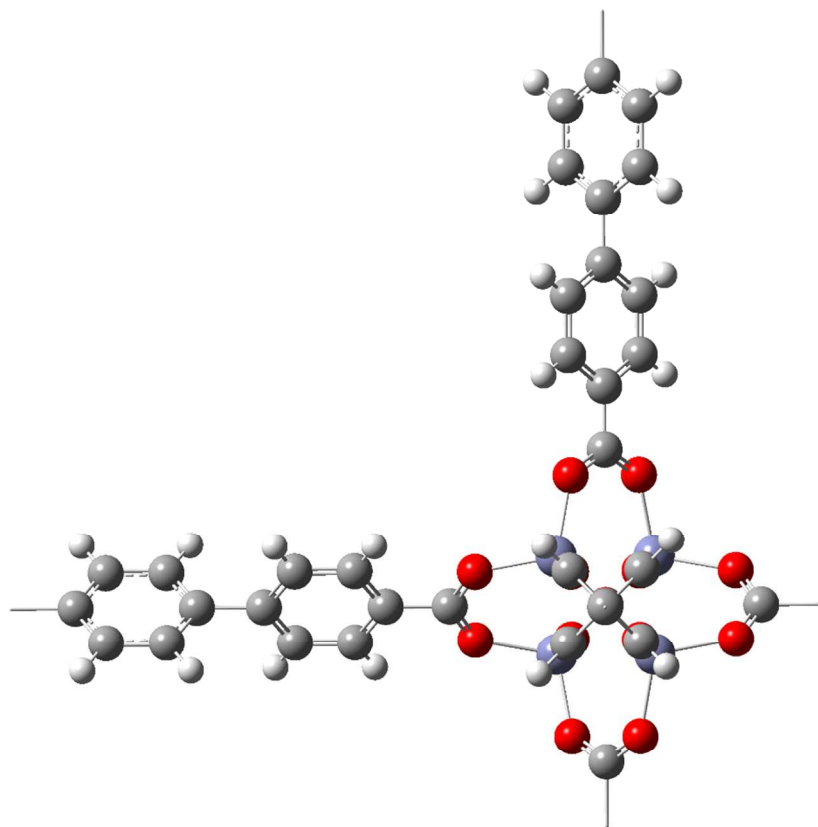


Figure 2. IRMOF model used in ab initio MD. 1,4-benzenedicarboxylate linkers of IRMOF-1 are substituted with 4,4'-biphenyldicarboxylate. The color representations are the same as in Figure 1.

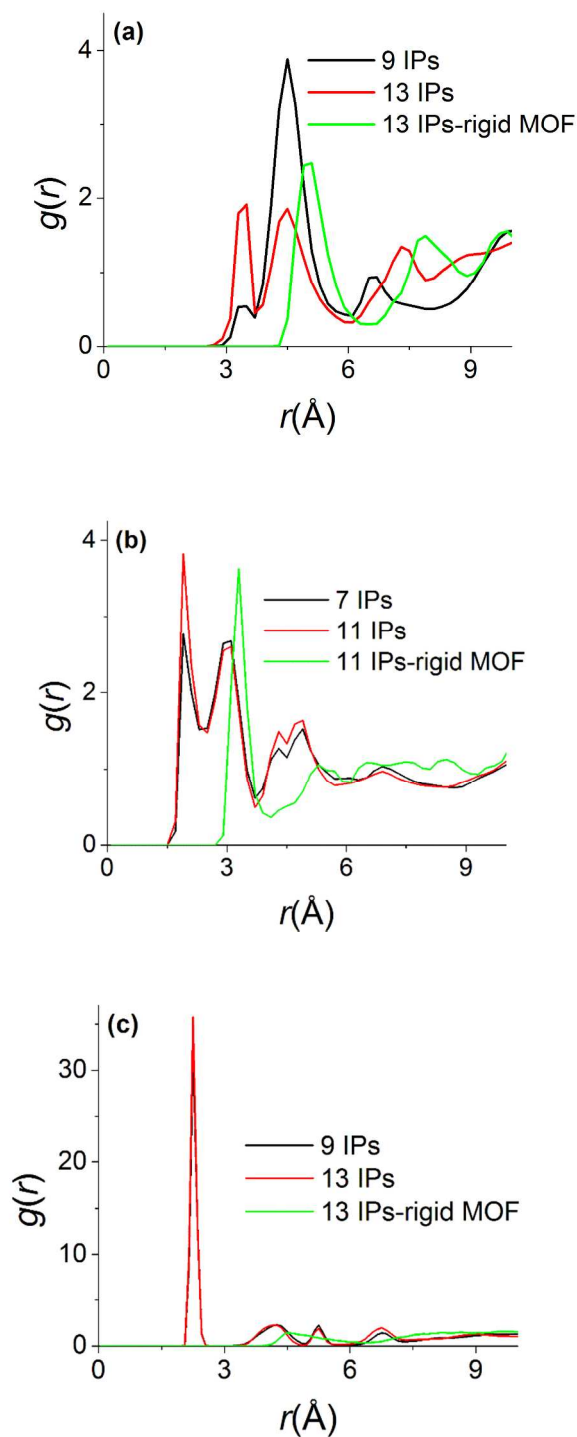


Figure 3. Radial distribution functions of anions of BMI^+ -based ILs around Zn of IRMOF-1: (a) P of PF_6^- , (b) O of Tf_2N^- and (c) Br^- . For each IL, the stable MOF cases with the largest number of ion pairs (cf. Table 1) and four fewer ion pairs are compared with the rigid MOF case.

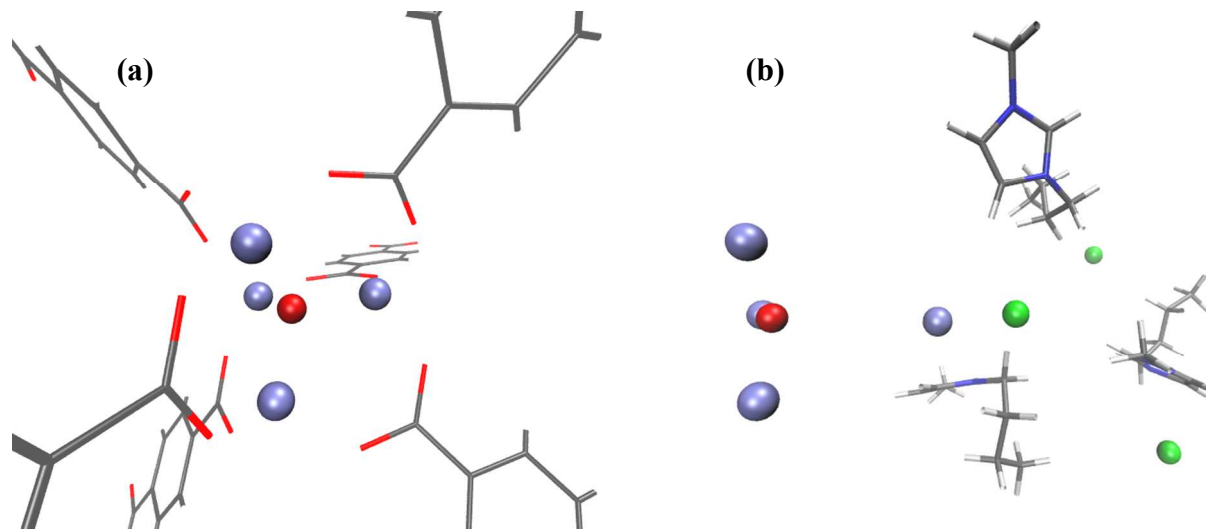


Figure 4. Molecular geometry of $\text{Zn}_4\text{O}(\text{1,4-benzenedicarboxylate})_6$: (a) crystal structure and (b) a snapshot taken from MD with 13 ion pairs of BMI^+Br^- present in the simulation supercell. For clarity, only three ion pairs closest to the Zn_4O site are shown and linkers are not displayed in (b). The interactions of Br^- (green) with Zn (purple) deform the metal site, Zn_4O , from its tetrahedral symmetry (panel (a)) by pulling a Zn atom towards the MOF cavity (panel (b)). Analysis shows that the distance between the displaced Zn and the central O (red) in (b) can reach 4.5 Å (the corresponding distance in the crystal structure in (a) is 1.93–1.95 Å). Three other zinc atoms that are not displaced become nearly co-planar with the central O as shown in (b). Despite its significant structural disruption, MOF was found to be stable in this case according to MD (see Table 1).

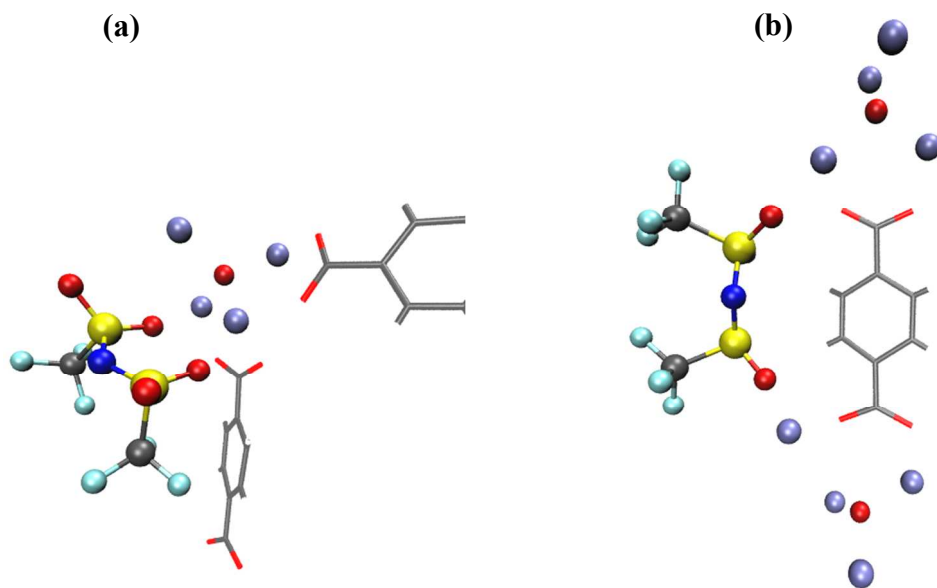


Figure 5. Two frequently-occurring configurations of TF₂N⁻ near Zn₄O groups: a single anion interacts with (a) one and (b) two Zn₄O groups. Color: S (yellow), O (red), C (dark gray), N (blue), F (light green), and Zn (purple).

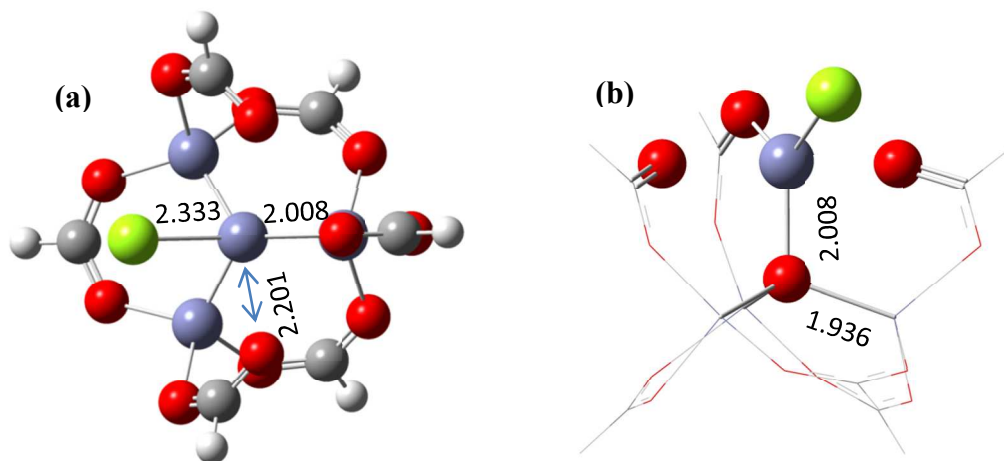


Figure 6. Optimized molecular structure of $\text{Zn}_4\text{O}(\text{HCO}_2)_6$ in the presence of one bromide anion. Two different views of the structure are shown in (a) and (b). In (b), Br^- interacting with Zn and its coordinated O atoms form a trigonal bipyramidal structure with the base consisting of two O atoms and Br^- . The Zn atom is nearly co-planar with the base. See Figures 1 and 4 for color representations of different atom types. Distances are measured in units of Å.

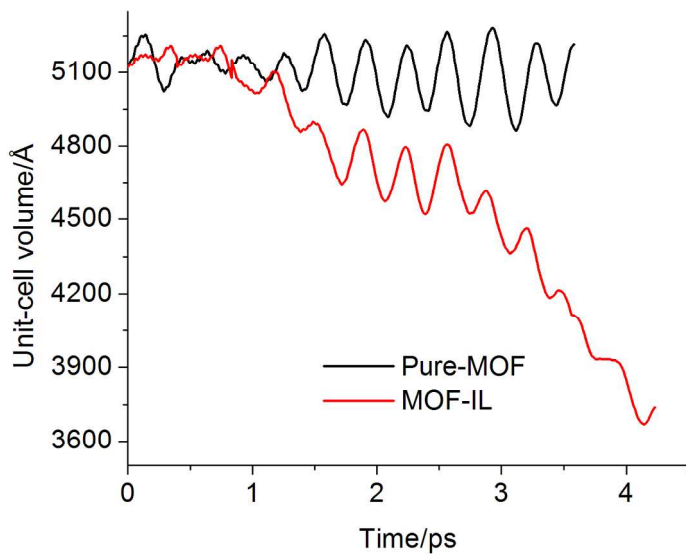


Figure 7. AIMD results for temporal changes of the unit-cell volume of the model IRMOF system (Figure 2) in the absence and presence of a guest DMI^+Br^- ion pair.